PERGAMON

Journal of Structural Geology 23 (2001) 1549–1565

JOURNAL OF STRUCTURAL GEOLOGY

www.elsevier.com/locate/jstrugeo

Strain in ductile shear zones in the Caledonides of northern Sweden: a three-dimensional puzzle

P. Bhattacharyya*, P. Hudleston

Department of Geology and Geophysics, University of Minnesota, Minneapolis, MN 55455, USA

Received 25 February 2000; revised 23 January 2001; accepted 30 January 2001

Abstract

Small-scale ductile shear zones are well developed in amphibolites of Caledonian nappes of the Swedish Lapland. Strain in the shear zones is recorded by the shapes of originally sub-equant aggregates of plagioclase feldspar. Classical strain analysis on two-dimensional (*xz*) profiles across the shear zones leads to results that indicate large volume losses associated with the shear strain. Large volume losses are, however, incompatible with geochemical analysis, which shows little chemical variation across the shear zones. By including data from *xy* and *yz* sections, information on the three-dimensional state of strain can be obtained. These data indicate that deformation is not confined to a two-dimensional plane—particle extension within the shear zone, parallel to the shear plane and perpendicular to the shear direction has also occurred. The state of strain and strain path in the shear zone can be modeled in a general way by combining stretches in *x*, *y* and *z* with simple shearing and volume loss. End member models correspond to plane strain with volume loss ($k_X = k_Y = 1$; $k_Z < 1$), 'transpression' ($k_X = 1$; $k_Y = 1/k_Z$), and pure shear ($k_X = 1/k_Z$; $k_Y = 1$). These models produce identical strain ratios and orientations on the *xz* section, but differ in stretch in *y* and in area of the strain ellipse on the *xz* section. Extension in *y* or *x* allows for reconciliation of the geometrical and geochemical data for part of an individual shear zone, but poses a problem of strain compatibility at the edges and terminations of the shear zones. The shear zones show a complex anastomosing pattern in three dimensions, and their connectivity provides a way in which strain compatibility is maintained.

Keywords: Ductile shear zones; Shear strain; Transpression

1. Introduction and background

Ductile shear zones provide valuable information for studying progressive non-coaxial deformation in rocks and a means of correlating rock fabric with strain (e.g. Ramsay and Graham, 1970; Hudleston, 1977; Lister and Williams, 1979; Simpson, 1983; Law, 1990; Lloyd et al., 1992; Mohanty and Ramsay, 1994). Based on the model of shear zones proposed by Ramsay and Graham (1970), it is often assumed that, for a shear zone with monoclinic symmetry, the deformation is restricted to the plane perpendicular to the shear plane and parallel to the shear direction. It is also commonly assumed that the wall rocks remain free from deformation. This geometry, for a sinistral ductile shear zone, is schematically shown in Fig. 1, in which the *xy*-plane is the shear plane, and *x* is the shear direction. For such an ideal shear zone, the deformation can only be accommodated by heterogeneous simple shear and/or heterogeneous volume change across the shear zone, the two operating in tandem or one finite deformation sequentially following the other (Ramsay and Graham, 1970). In addition, there is the possibility of adding an arbitrary homogeneous strain affecting the shear zone and wall rock alike. The simple shear and volume change components in an ideal shear zone can be determined solely on the basis of finite strain analysis on the *xz*-plane of Fig. 1 (e.g. Ramsay, 1980; Mohanty and Ramsay, 1994).

In a number of studies, analysis of strain assuming the band model of Ramsay and Graham (1970) has led to the conclusion that large volume losses are associated with the development of ductile shear zones (e.g. Mawer, 1983; Mohanty and Ramsay 1994; Srivastava et al., 1995). Such a conclusion has been greeted with skepticism by some workers (e.g. Schwerdtner, 1982; Mawer, 1983), and this skepticism is supported by geochemical analyses, which indicate little or no changes in chemistry across shear zones, in cases in which protolith can be assumed with confidence (e.g. Simpson, 1983; Srivastava et al., 1995). It is not conceivable that volume loss in a deforming rock can be achieved without differential mobility of elements. This then gives rise to a paradox: geometrical analysis leads to

* Corresponding author.
E-mail address: bhat0018@tc.umn.edu (P. Bhattacharyya).

0191-8141/01/$ - see front matter
PII: S0191-8141(01)00020-7

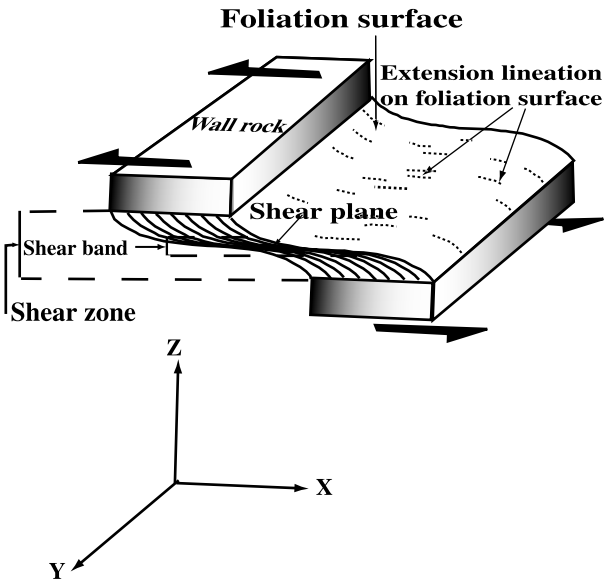

Fig. 1. Schematic representation of the geometry of a sinistral ductile shear zone or shear band assuming the model of Ramsay and Graham (1970). Various associated structures are also shown. The co-ordinate system used here to describe the shear zone is indicated. Modified from Hanmer and Passchier (1991). Note that the reference frame used to describe the kinematics of deformation (x, y, z) is not the same as the reference frame used to define the finite strain (X, Y, Z).

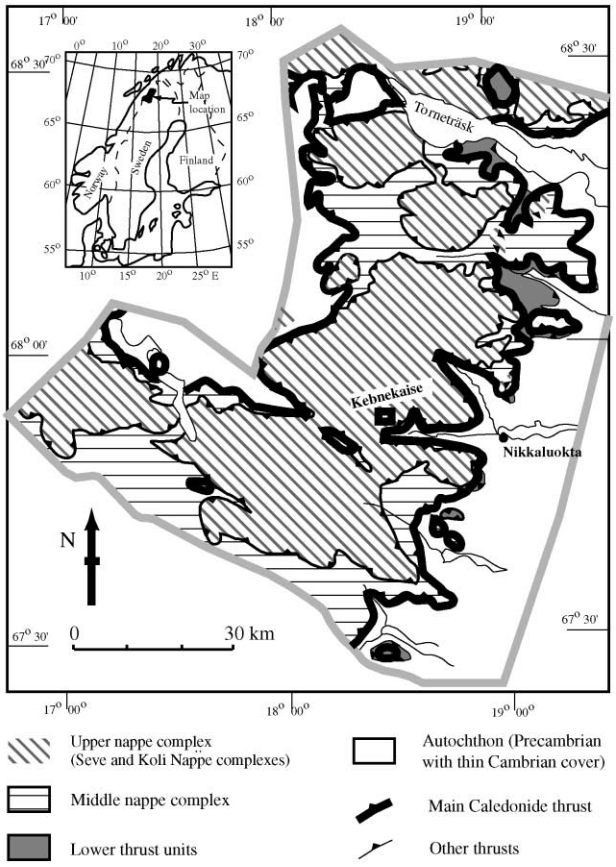

Fig. 2. Simplified geological map of the area around Kebnekaise, northern Sweden (modified after Kulling (1964) and Srivastava et al. (1995)). The sample location is shown by a rectangle near Kebnekaise.

the conclusion that strain in ductile shear zones is accompanied by large volume losses, whereas geochemical analysis leads to the conclusion that volume loss is at best minimal.

The resolution of this paradox in all likelihood lies in considering the three-dimensional geometry of shear zones. All shear zones deviate from ideal monoclinic symmetry to some degree. The walls of shear zones are typically neither exactly straight nor parallel, and shear zones, like faults, have terminations or tip lines (Coward, 1976; Ramsay, 1980, fig. 17; Coward and Potts, 1983). Also, shear zones are often found in an anastomosing pattern in three dimensions, with the same or opposite senses of displacement on intersecting zones (Ramsay and Allison, 1979; Choukroune and Gapais, 1983; Simpson, 1983; Gapais et al., 1987). Therefore, a two-dimensional model of shear-zone deformation will not be appropriate for many ductile shear zones, and may lead to misleading conclusions about the nature of deformation within individual zones. Specifically, this is the case concerning volume loss in the shear zones that we have studied and described here.

It can reasonably be assumed that progressive deformation under natural conditions involves some combination of simultaneous pure shearing and simple shearing (the '-ing' suffix used here indicates the kinematic aspect of deformation as suggested by Means, 1990), with or without progressive volume change (e.g. Passchier and Urai, 1988; Wallis, 1992; Fossen and Tikoff, 1993; Tikoff and Teyssier,

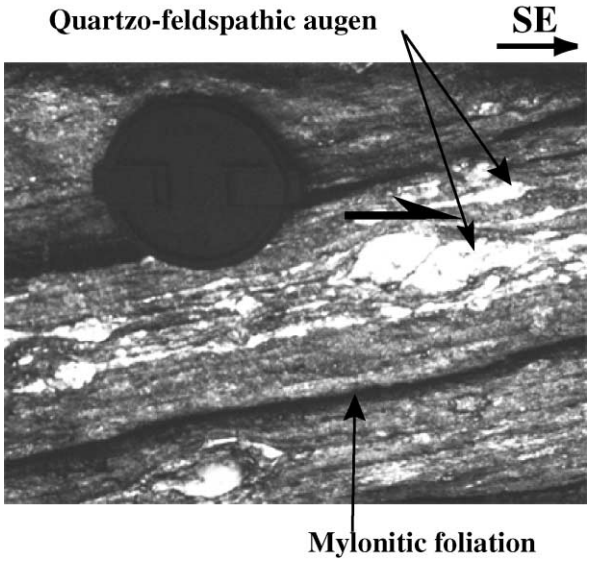

Fig. 3. Field photograph of a subvertical outcrop, showing piggyback structure exhibited by quartzofeldspathic augen indicating top-to-the-southeast sense of movement.

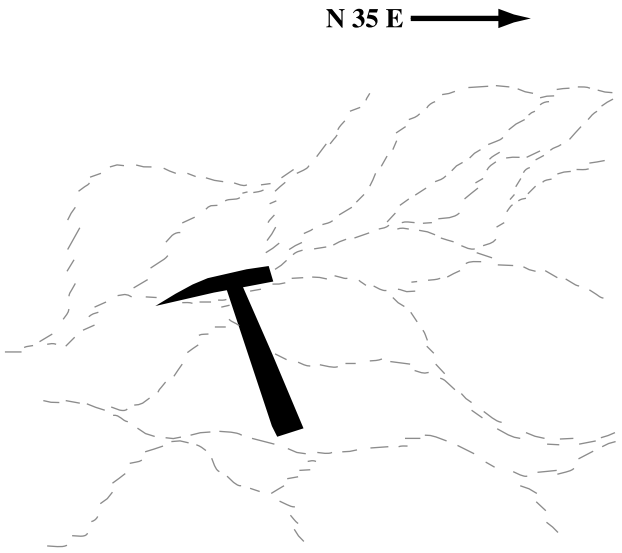

Fig. 4. Field sketch showing anastomosing shear geometry on a two-dimensional subvertical outcrop. The regional foliation dips gently towards the northwest. The outcrop is subperpendicular to the trend of the regional lineation.

1994). In such cases, a component of pure shear acting perpendicular to the shear plane (*xy*-plane of Fig. 1) should also be accounted for. As pointed out by Tikoff and Fossen (1993), such a component of shortening generally gives rise to a loss of area of the strain markers on the *XZ* principal plane, and also affects the orientation and aspect ratio of strain markers on this plane, giving the impression of volume loss. Thus, a two-dimensional fabric analysis on the *XZ*-plane (Fig. 1) alone can lead to erroneous conclusions regarding volume change.

In order to investigate the problem further, we have conducted three-dimensional strain analyses on several samples of amphibolite containing well-defined ductile shear zones. These samples are from the same rocks studied by Srivastava et al. (1995), who described a shear zone that exemplifies the 'volume-loss paradox'. A description of the samples is provided below and then a brief outline of the mathematical basis for the analysis that follows.

In this work, the term 'shear zone' or 'shear band' is used to imply a region of heterogeneously deformed rock, in which the deformation progressively increases towards the center. It is a relatively narrow zone defined by sub-parallel, planar boundaries (Fig. 1).

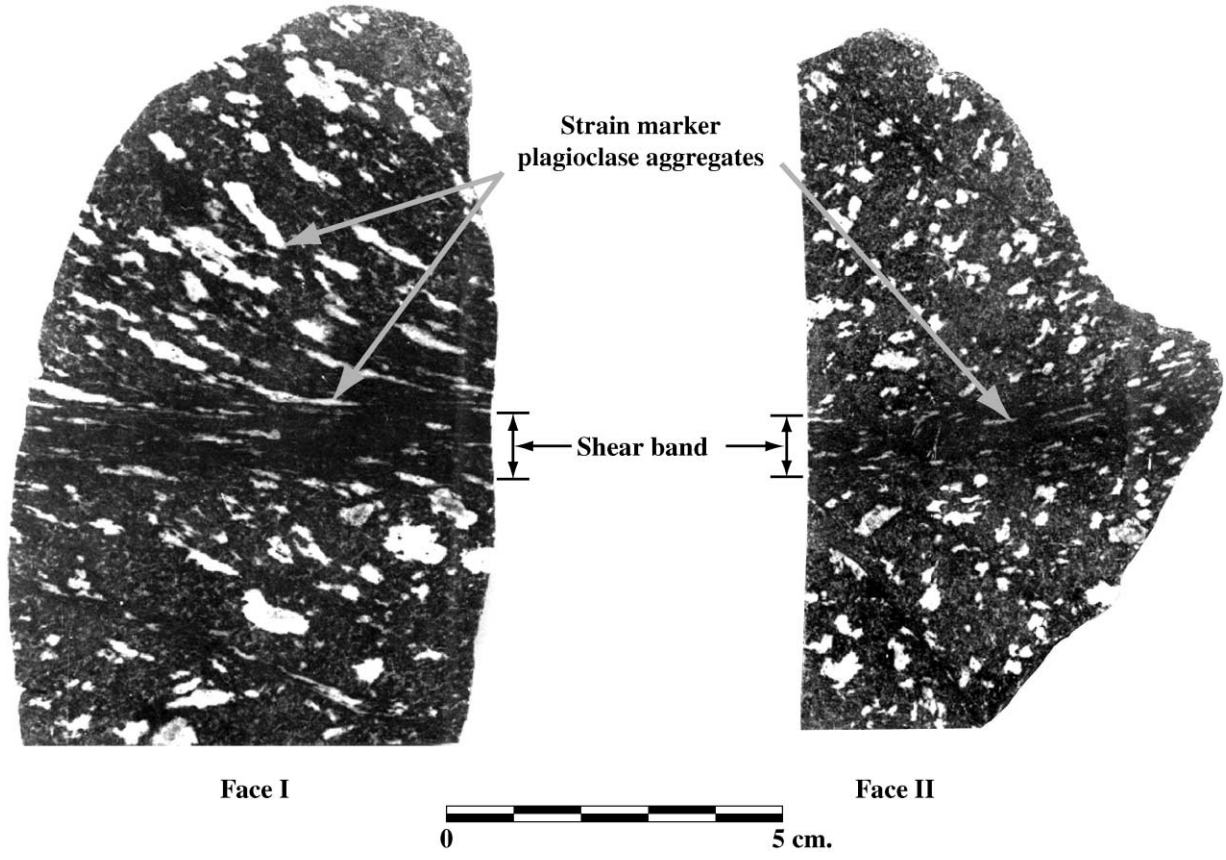

Fig. 5. The digitized images of two perpendicular sections of sample I. The shear band boundaries are defined by sub-parallel, highly elongate feldspar aggregates. The deformation fabric is asymmetrical on either side of the shear band, as can be seen from Face I.

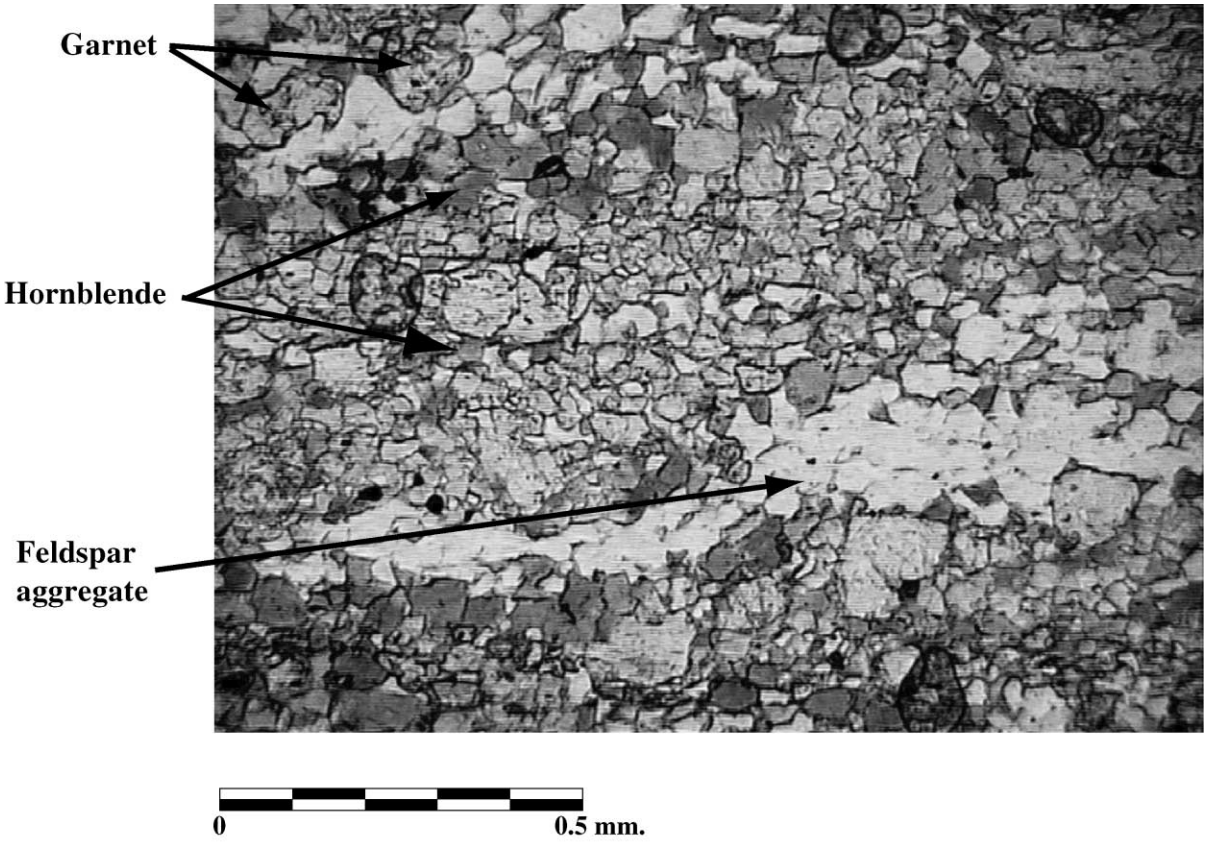

Fig. 6. Photomicrograph under plane-polarized light showing representative textural and mineralogical features within the shear zones. The straight, sharp grain boundaries and triple junctions among the major mineral phases indicate closeness to equilibrium.

2. Geological setting and sample description

The shear zones under study are developed in meta-gabbros or amphibolites exposed in the vicinity of Kebnekaise in Swedish Lapland. These rocks were identified by Srivastava et al. (1995) as part of the Eastern Amphibolites, belonging to the Seve Nappe Complex of the Upper Allochthon of the northern Scandinavian Caledonides (Gee and Zachrisson, 1979; Gee et al., 1985). The nappes were thrust from west to east to overlie thin Cambrian strata and basement rocks of the Baltic Shield (Gee and Zachrisson, 1979). Geological mapping by the authors in the Kebnekaise area (Fig. 2) has shown that the shear zones occur most prominently in an overall rather massive garnet amphibolite within the Kebne Dyke Complex of Andréasson and Gee (1989) which, according to Dallmeyer et al. (1991), intruded the thinned and rifted Baltoscandian passive margin during the late Proterozoic (~650–600 Ma), and was tectonically emplaced during the Finnmarkian orogeny (520–500 Ma).

Regionally, foliation has a gentle but variable west-northwesterly dip of about 20°, sub-parallel to the boundaries of lithotectonic units. Where foliation is strongly developed, it may be affected locally by small- to medium-scale folds, from tight to isoclinal and generally intrafolial.

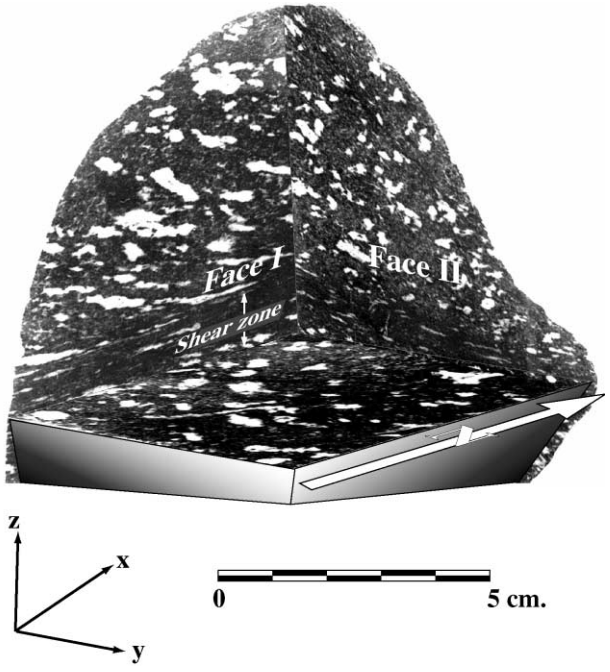

Fig. 7. The spatial relationship of the three mutually perpendicular sections of sample I. The arrow indicates the frame of reference used in constructing the strain ellipsoids.

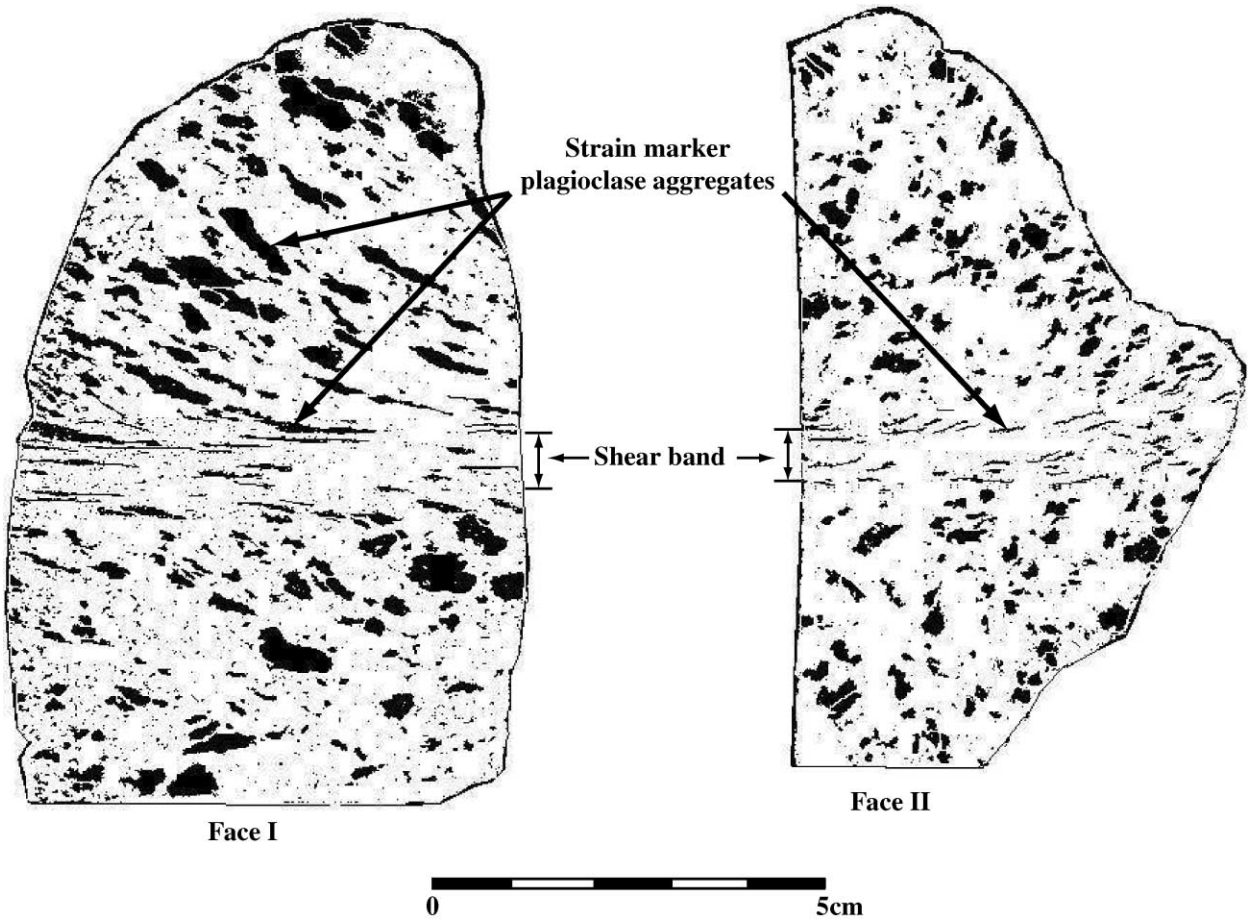

Fig. 8. Binary images of Faces I and II shown in Fig. 5.

Lineation is defined by aligned hornblende, a linear mylonitic fabric element, and elongated plagioclase aggregates (the latter especially within the Kebne Dike complex). The average plunge of lineation is about 20° to the west-northwest (i.e. down the dip of the foliation), with a top-to-the-southeast sense of movement, as exhibited by asymmetric shear sense indicators (Fig. 3). The shear zones occur in three-dimensional arrays (an example of these in two-dimensional section is shown in Fig. 4), with regions between individual shear zones of little or no strain. Both the planar and linear fabric elements in individual shear zones and the arrays themselves are consistent with the regional pattern of foliation and lineation in the surrounding rocks, which suggests that the shear zones developed as part of the tectonic processes that resulted in nappe emplacement. The precise role played by the shear zone arrays in the regional thrust emplacement event, however, remains uncertain, and is the subject of additional study.

In hand specimens, the amphibolites possess a variably-developed foliation defined by aggregates of recrystallized plagioclase feldspar (Fig. 5). The shear bands appear as zones in which the feldspar aggregates are much more elongate than in the adjacent rock, the aggregates becoming

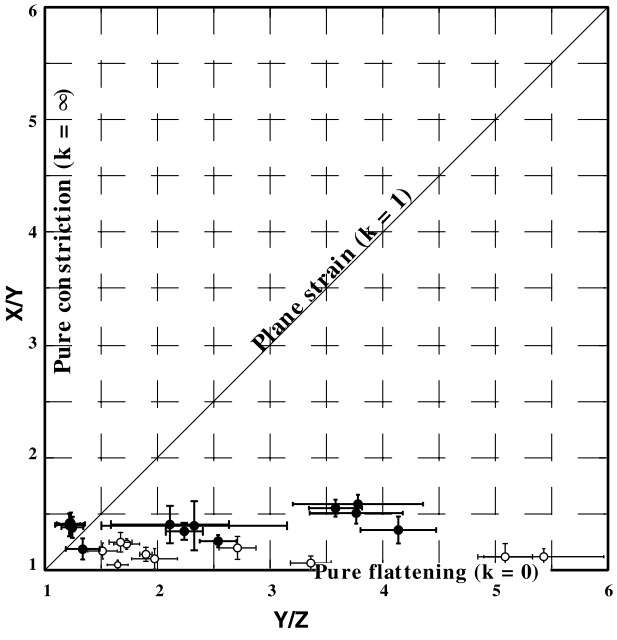

Fig. 9. The geometry of the strain ellipsoids calculated for samples I and II are plotted on a Flinn diagram. *X*, *Y* and *Z* are principal strains. Data from sample I are shown as solid circles. Data from sample II are shown as open circles.

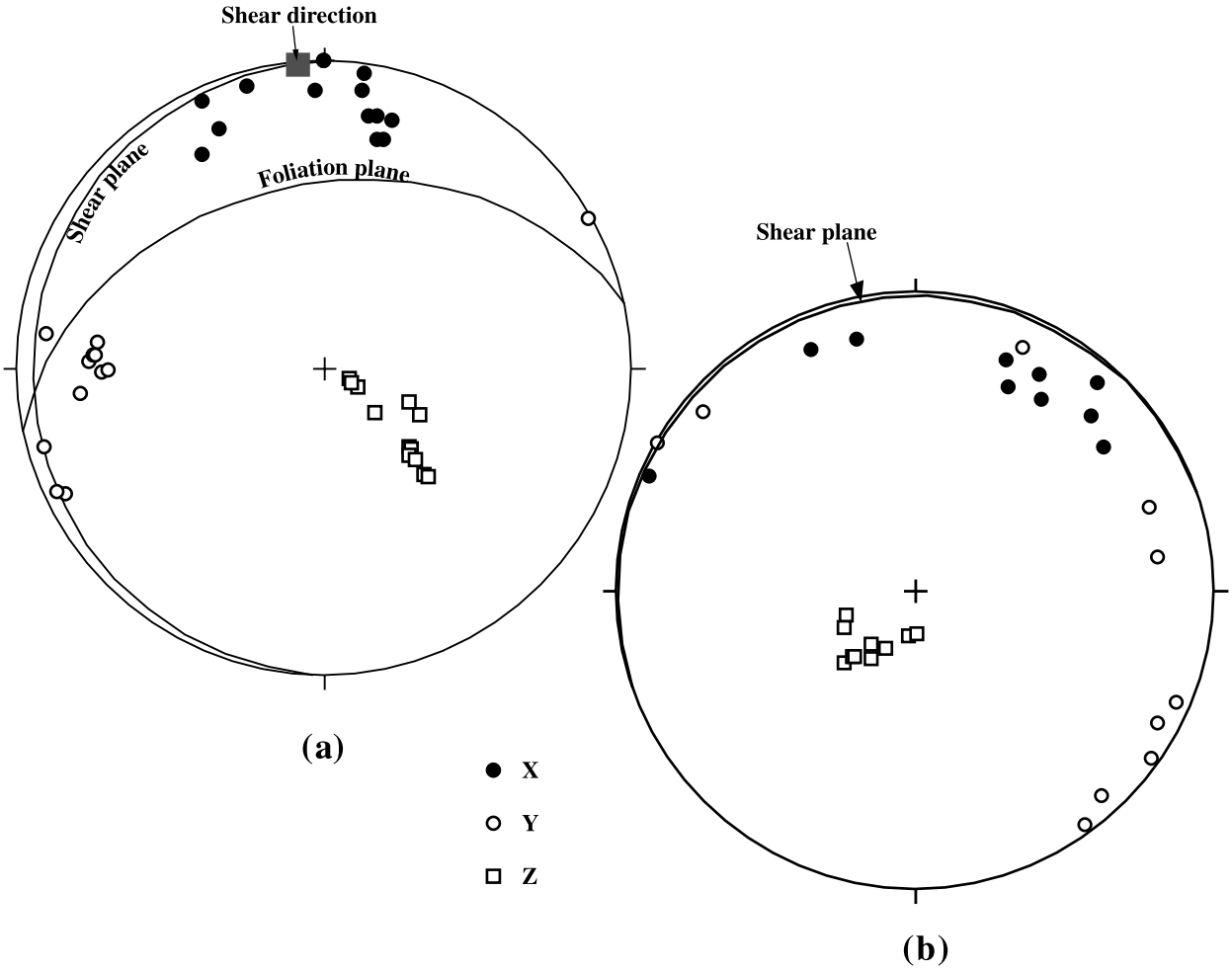

Fig. 10. Equal-area projections showing the orientations of the principal directions of the calculated strain for sample I (a) and sample II (b). Solid circles, *X*-direction; open circles, *Y*-direction; open squares, *Z*-direction. The orientations of the shear plane, foliation plane and shear direction are included in (a) and the shear plane is indicated in (b).

progressively more elongate towards the centers of zones. In the samples studied, the shear zone boundaries are sub-parallel (Fig. 5), although the length of the shear zones exposed in these samples is not great. Within the centers of the shear bands, the feldspar aggregates may effectively 'disappear', or become so attenuated that they are indistinguishable from the matrix, thereby making strain indeterminate in the most highly deformed rocks. The shear zones are typically 10–50 mm in width, and in three dimensions either die out or, more commonly, connect in some way to another shear zone (Fig. 4).

A weak grain-shape fabric with a preferred alignment oblique to the plane of shear has been identified by Srivastava et al. (1995) using the SURFOR wheel method of Panozzo (1987). The alignment is consistent with the sense of shear indicated by the feldspar aggregates. No evidence of necking or boudinaging of individual feldspar aggregates can be detected, even at aspect ratios in excess of 20:1. Also, the weak grain-shape fabric shows no tendency to be deflected at the borders of the aggregates. Hence, it is assumed that there was little or no viscosity contrast between the feldspar aggregates and the groundmass, and therefore that the aggregates can be used as passive strain markers.

In thin section, the rock is mainly composed of polygonal grains of hornblende, quartz, garnet, plagioclase feldspar and clinopyroxene (diopside), with minor amounts of zircon, rutile, apatite, titanite, zoisite and sulphides (e.g. pyrite) (Fig. 6). The near equigranular, equidimensional texture with sharp grain boundaries and triple junctions among all major mineral phases indicates a close approach to textural equilibrium (Fig. 6). Mineralogy, texture and grain size within and outside the shear zones are similar. Most of the quartz grains (>95%) within the shear zone do not exhibit undulose extinction and possess straight grain boundaries. These features indicate that recovery processes and annealing overprinted most of the effects of strain within the shear zone. Hence, the shearing event was either synchronous with or outlasted by the peak metamorphic event, during which such recovery processes were dominant.

Srivastava et al. (1995) determined that the sheared rocks

were metamorphosed at about 800°C, based on garnet–clinopyroxene (Powell, 1985) and garnet–hornblende (Graham and Powell, 1984) paleothermometry, and pressures of 9–14 kb, based on garnet–clinopyroxene–plagioclase–quartz (Moecher et al., 1988) and garnet–hornblende–plagioclase–quartz (Kohn and Spear, 1989) paleobarometry. These *P–T* conditions indicate upper amphibolite to granulite facies metamorphism, and thus it was concluded by Srivastava et al. (1995) that the deformation within these shear zones occurred near the base of the crust, if of normal thickness. Further studies of the metamorphic mineral assemblages corroborate these results (Bhattacharyya et al., 1999).

3. Analytical techniques

3.1. Three-dimensional strain determination

A 'shear plane' and 'shear direction' for each of the shear zones in several samples were identified based on the geometry of the deformed feldspar aggregates. The procedure for doing this follows Hudleston (1977) and Srivastava et al. (1995). It is not necessary to assume that the stretching lineation indicates the shear direction, only that the latter is in the shear plane perpendicular to the axis about which the foliation in the shear curves. In what follows, the shear plane is arbitrarily assumed to be horizontal, and the shear direction aligned north–south. We conducted fabric analyses on three mutually perpendicular sections of each sample, and one of these sections was cut parallel to the shear plane (*xy*-plane of Fig. 1). The second section was cut in the plane perpendicular to the shear plane that shows the maximum curvature of the foliation plane. This section thus contains the local shear direction: it is a vertical face striking north. The third section is cut perpendicular to the first two, making it parallel to the *yz*-plane of Fig. 1. The spatial relationships of the three sections for one sample (sample I) are shown in Fig. 7. Zones of approximately homogeneous strain were visually identified based on the curvature of the foliation plane, and several more sections parallel to the shear plane were cut approximately at the boundaries between those zones. Thus for each sample, several zones of approximately homogeneous strain were obtained in a three-dimensional array. The shapes of the plagioclase aggregates on each section were used to carry out fabric and strain analyses. The contrast between aggregate and matrix on digitized photographic images (Fig. 8) of the polished rock sections was sufficient to allow standard image analysis techniques to be used for the purpose of defining aggregates and determining their shapes and orientations. The results of analyses of two samples (I and II) are presented here, together with geochemical analyses of one of these samples (II) and of a third sample (III).

The shape fabric data collected from each set of three two-dimensional planes in each of the samples were combined by means of the software MacStrain (Kanagawa, 1990). Three-dimensional finite strain information was thereby obtained following the tensor algebraic method of Wheeler (1986). Thus, from sample I, we obtained 13 finite strain ellipsoids at different positions across the shear zone (Figs. 9 and 10). Ellipsoids 1–6 are for zones lying above the shear band, ellipsoids 7–10 are within the shear band, and ellipsoids 11–13 are from below the shear band. Similarly, we obtained 10 ellipsoids for sample II.

The shapes of the strain ellipsoids obtained for samples I and II are plotted on Flinn diagrams in Fig. 9 (the major-, intermediate- and minor-axes of the finite strain ellipsoid are referred to here as *X*-, *Y*- and *Z*–axes, respectively). The orientations of the principal axes of these ellipsoids are plotted in Fig. 10a and b. The cuts in the samples were not perfectly parallel to the shear plane (*xy*-plane of Fig. 1) and, once cut, the orientations of the shear plane (182/6W for sample I and 251/2N for sample II) were measured on the respective samples independently. They also are plotted in Fig. 10a and b. In addition, the orientation of the foliation plane (258/40N) making the maximum angle with the shear plane was measured directly on sample I and is plotted in Fig. 10a. The orientation of the 'shear direction' (1/355) for sample I was thereby determined as being the line lying in the shear plane and perpendicular to the line of intersection between the shear plane and the measured foliation plane (Fig. 10a).

It is apparent from Fig. 9 that the strain in the two shear zones studied is generally of strongly flattening type (pure flattening is given by Flinn's $k = 0$), with sample II showing

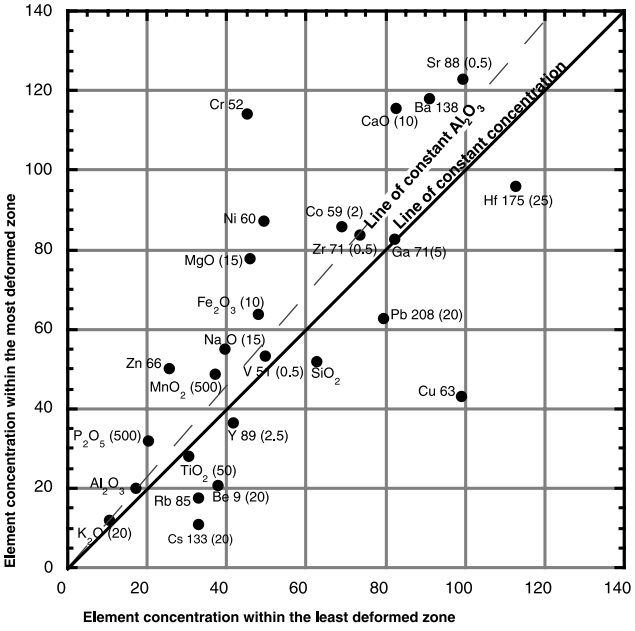

Fig. 11. An isocon diagram (Grant, 1986) comparing concentrations of selected elements within the most deformed zone to those from the least deformed zone of sample III. Element labels and the scaling factors (within parentheses) for each element are provided. Otherwise concentration is in weight percent.

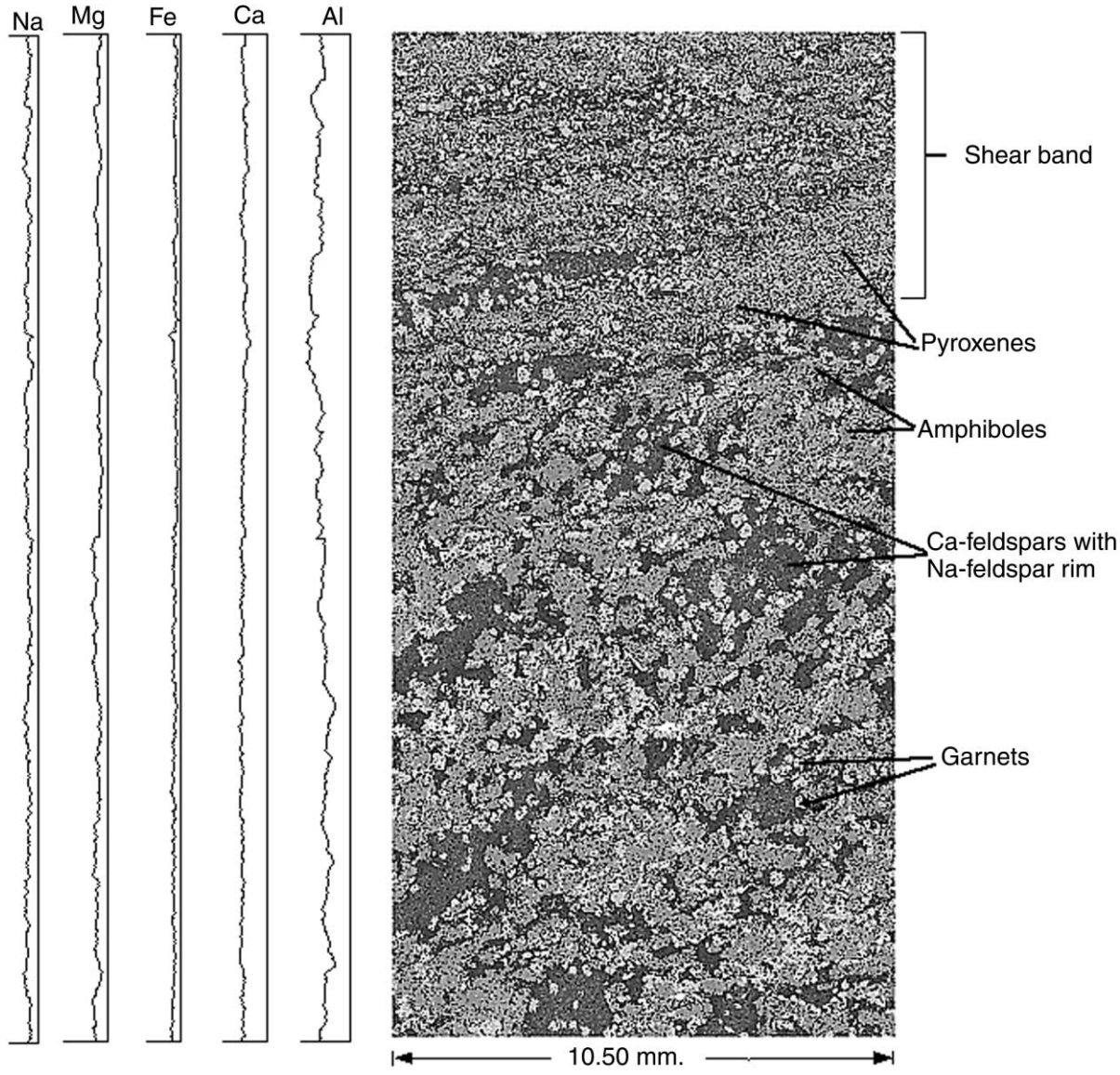

Fig. 12. Backscattered image of a polished thin section parallel to the 'North' face of sample II. The feldspar aggregates can be identified on the basis of the intensity of the grayscale values. The profile sections for Ca, Al, Mg, Na and Fe, showing their concentrations across the shear band in sample II, are also shown.

stronger flattening and larger variation than sample I. The weakly strained parts of the sample I cluster near the origin of the Flinn plot, and the most strongly deformed parts, in the centers of the shear zones, lie much closer to the line $X/Y = 1$ ($k = 0$), than the line $X/Y = Y/Z$ ($k = 1$). If the data collectively can be considered to represent a deformation path, it would clearly be one with a strong component of flattening.

The principal directions of the calculated strain ellipsoids are consistent with the geometry of the shear plane and shear direction determined from bulk rock fabric. The directions of minimum stretch, Z, lie at a high angle to the shear plane, and the directions of maximum stretch, X, lie at a low angle to the shear plane, with deviations from perpendicularity and parallelism being least for the most strongly deformed parts of the shear zone (Fig. 10a and b). The Y directions of strain in sample I cluster around the intersection of the shear plane and plotted foliation plane (Fig. 10a); the X and Y directions of sample II are broadly dispersed along the shear plane (Fig. 10b), consistent with a strain symmetry of close to pure flattening type—in which neither X nor Y is well defined (as apparent from the Flinn plot in Fig. 9).

3.2. Geochemical analysis

Whole rock geochemical analysis was conducted on sample III by means of inductively coupled plasma–mass spectrometry (ICP–MS), with an ELAN 5000 from Perkin Elmer/Scitex in the Department of Geology and Geophysics

at the University of Minnesota. Sample III is similar to samples I and II in mineral composition and geometry, but more readily provides the sub-samples necessary for this type of analysis. The concentrations of oxides of selected elements from within the most deformed part of the sample are plotted against those of the same oxides from the least deformed part of the sample (Fig. 11). Grant (1986) has shown that, on such a plot, a straight line through the origin represents an 'isocon', such that all points on the line represent components whose concentrations are changed by the same factor. If there is no change in chemical composition between the most and least deformed parts of the sample, the points on an isocon plot will all lie on a straight line of slope 1. Immobile elements plotting above the line of unit slope indicate volume loss, whereas immobile elements plotting below this line indicate volume gain. Using the equations from Gresens (1967) and Grant (1986) has shown that the change in concentration of an individual rock component can be determined from the difference in slope of the isocon for that component and the 'isocon' of components that have remained immobile. Change in volume of the rock can be calculated in the same way. Most of the major elements and likely immobile elements lie close to the line of unit slope in Fig. 11, which is consistent with the rock having experienced little or no volume change, and thus elemental differentiation, associated with deformation in the shear zone. The isocon for constant Al_2O_3 (assuming Al_2O_3 to be immobile) is shown in Fig. 11, as well as that for constant mass (isocon with a slope of 45°). If Al_2O_3 was immobile, its isocon on Fig. 11 would indicate a volume decrease of $<15\%$.

The whole-rock geochemical analysis was complemented by element mapping on sample II with a JEOL 8900 electron microprobe in the Department of Geology and Geophysics at the University of Minnesota. Polished thin sections were made of the same three rock sections of sample II for which aggregate shape fabrics were analyzed. The concentrations of Ca, Al, Mg, Na and Fe were mapped using EDS techniques over an area containing the shear band for each of the polished thin sections. Each map measured 10.5 mm × 21 mm, taken at 20.2 nA probe current, 15 kV and 30 ms dwell time. Each element map was constructed on a 0–256 color scale. Using standard image-analysis procedures, profile sections for each of these maps were constructed by averaging the pixel values along each individual row (width = one pixel) of the maps. The profile sections for each of the five selected elements are shown in Fig. 12. The backscattered image obtained from the polished section made parallel to the vertical plane striking 'North' in sample II is also shown in Fig. 12 to demonstrate the relationship of the profile section plots with distance from the shear band. The profiles of the five elements show little indication of change in concentration as the shear zone is traversed; only Al concentration seems to be slightly elevated within the shear zone, indicating probable minor volume loss ($<15\%$). This is consistent with the data presented in Fig. 11, supporting the notion of little element mobility.

4. Analysis of results

4.1. Mathematical background for strain analysis

The strain in the shear zones studied is three-dimensional and, in analyzing our data, it is appropriate to consider the theoretical pattern of three-dimensional strain in a planar deformation band. We follow here the analysis of Fossen and Tikoff (1993) and Tikoff and Fossen (1993). Their equations for simultaneous superposition of pure shearing and simple shearing of a continuous body in three-dimensions were originally derived by Ramberg (1975a), and later expanded to include progressive volume change (Fossen and Tikoff, 1993; Tikoff and Fossen, 1993). The general equation representing the finite deformation matrix **D** due to simultaneous pure shearing and simple shearing, with or without progressive volume change in three dimensions

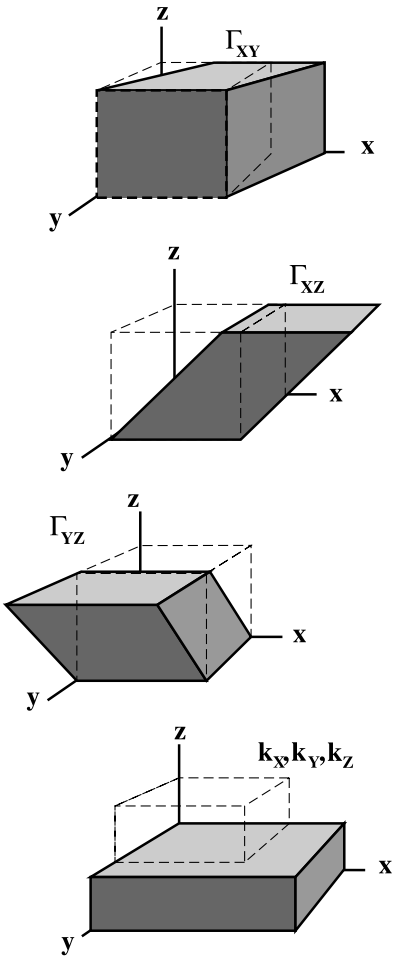

Fig. 13. Diagram of the different types of deformation described by the three-dimensional matrix (Eq. (1)). Modified after Fossen and Tikoff (1993).

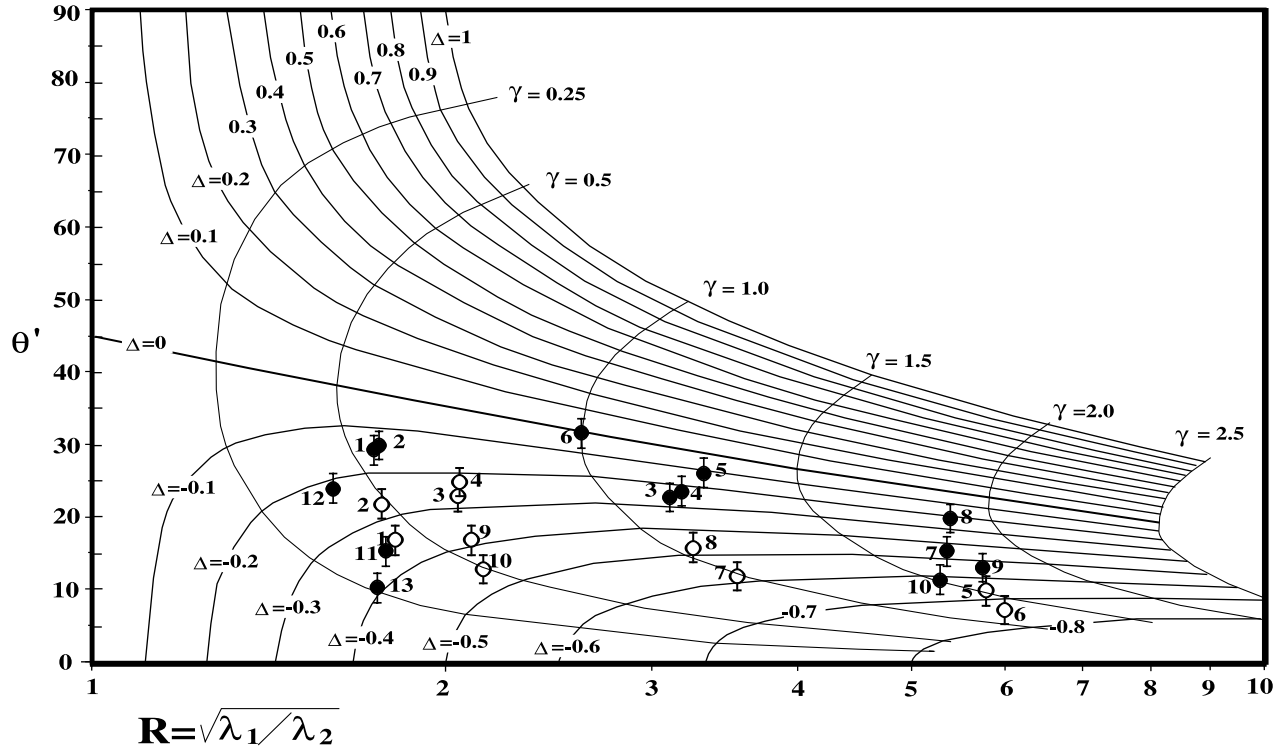

Fig. 14. The strain magnitude $R = \sqrt{\lambda_1/\lambda_2}$ ($\lambda_1 = X$, $\lambda_2 = Z$), plotted against the orientation (θ') of X on the XZ-principal plane for each finite strain ellipsoid constructed for both samples I and II. Also plotted are the two-dimensional theoretical curves representing simultaneous simple shearing and volume change (Tikoff and Fossen, 1993). Solid circles represent data from sample I. Ellipsoids 1–10 exhibit a regular progression from low to high strained state. Ellipsoids 11–13 do not follow this progression due to the asymmetry of the shear zone in sample I. Open circles represent ellipsoids 1–10 from sample II, which show a regular progression from low to high strain.

(Fossen and Tikoff, 1993, Eq. (17)) can be written as:

$$\mathbf{D} = \begin{bmatrix} k_x & \Gamma_{xy} & \Gamma_{xz} \\ 0 & k_y & \Gamma_{yz} \\ 0 & 0 & k_z \end{bmatrix} \tag{1}$$

where k_x, k_y and k_z represent the extensions or contractions along the x-, y- and z-coordinate axes, respectively (Fig. 13), and the off-diagonal terms (Γ_{ij}) represent effective shear strains. Volume change is given by the value of $|1 - k_x k_y k_z||1 - k_x k_y k_z|$. If the magnitude and orientation of the finite strain ellipsoid can be estimated from a ductile shear zone (e.g. Ramberg, 1975b; Owens, 1984; De Paor, 1990), the terms k_i and Γ_{ij} can in principle be calculated and the components of pure-shearing and simple-shearing, as well as the magnitude of associated volume change, can be assessed. In most cases, symmetry of deformation in the shear zone is utilized to simplify the analysis.

The finite deformation **D** can be achieved by the accumulation of successive equal strain increments of an arbitrary magnitude; this can be considered one way to represent a steady-state deformation path. The relationship between the incremental ($\mathbf{D}_{\text{incr.}}$), and the finite deformation matrix ($\mathbf{D}_{\text{total}}$) for steady state (Fossen and Tikoff 1993, Eq. (23)) can be expressed as:

$$\mathbf{D}_{\text{total}} = (\mathbf{D}_{\text{incr.}})^n \tag{2}$$

where n is the number of increments. The deformation path can thus be calculated for any particular finite deformation assuming steady state flow. It can be represented by plotting the n cumulative strains at each stage of the history. Thus Eqs. (1) and (2) form the basis of the mathematical treatment of strain partitioning and analysis of the deformation path in a ductile shear zone. It should be emphasized, however, that the 'general' deformation equation represents a homogeneous state of strain within the shear zone. It does not take into account strain gradients along a shear zone, or represent shear zones with non-parallel sides.

4.2. Two-dimensional modeling

For observations on our samples and other rocks from the region, in which metagabbros with equant feldspars and relict igneous textures can be found, it seems reasonable to assume that there is no preexisting strain fabric present in the rock. That is, we assume that outside the shear zones, the state of strain is zero.

Let us first consider deformation in the shear zone to be confined to the xz-plane (Fig. 1), with xy as the shear plane,

and x as the shear direction. Ductile shear zones are conventionally analyzed in this mode. Data from the xz-plane for our two samples are plotted in Fig. 14. On this plot, contours of shear strain and volume loss are plotted as intersecting sets of curves. All the data lie on or below the plane strain, simple shear line ($\Delta = 0$). They suggest volume losses of 0–75%, with volume loss generally increasing with strain intensity. For sample I (solid circles in Fig. 14), volume losses of up to 40% are indicated for low shear strains ($\gamma = 0.3$–0.6), and up to 60% at higher strains ($\gamma = 1.0$–1.8). For sample II (open circles in Fig. 14), volume losses of up to 45% are indicated for low shear strains ($\gamma = 0.4$–0.7), and up to 75% at higher strains ($\gamma = 1.0$–1.5). The average area of the feldspar aggregates on the xz-plane decreases towards the center of the shear zones (Fig. 15) and is consistent with the notion of volume loss. The strain distribution in sample I shows an asymmetry across the shear zone. On one side, strain increases fairly smoothly from the edge to the center of the zone (ellipsoids 1–10). On the other side, the low strain states (ellipsoids 11–13) lie off the trend set by ellipsoids 1–10.

The large volume losses that might be inferred from this analysis are incompatible with the geochemical data, and we next examine the problem as one of three-dimensional strain, in which we will show that there is no need for volume loss.

4.3. Modeling of possible deformation paths

As in the case of the two-dimensional modeling, we assume that outside the shear zones, the state of strain is zero. In addition, based on the results of geochemical analysis, we assume no volume change.

A modified version of the software program GENERAL SHEAR (Tikoff, pers. commun.) based on Eqs. (1) and (2) was used to model several possible deformation paths that could explain the observed three-dimensional fabrics associated with the shear zones in samples I and II. For this analysis, it was assumed that: (i) the calculated finite strain ellipsoids represent stages of homogeneous, steady-state deformation; (ii) the deformation involves some combination of simultaneous pure shearing and simple shearing with simple shear only in the x-direction (Fig. 1); and (iii) the deformation is associated with no progressive volume change. The deformation matrix (Eq. (1)) then

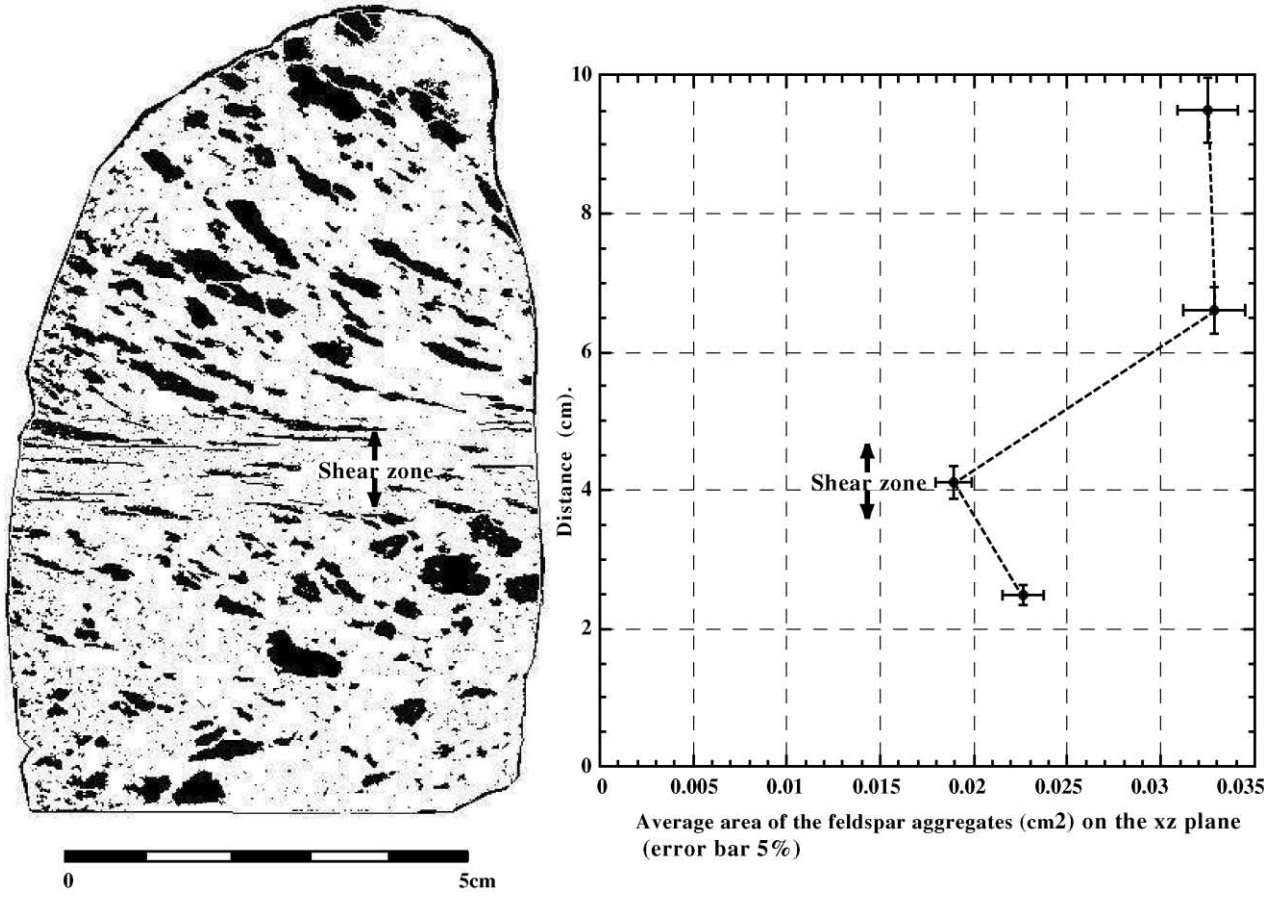

Fig. 15. Change in the area of the feldspar aggregates across the shear zone on the xz-plane are plotted for sample I.

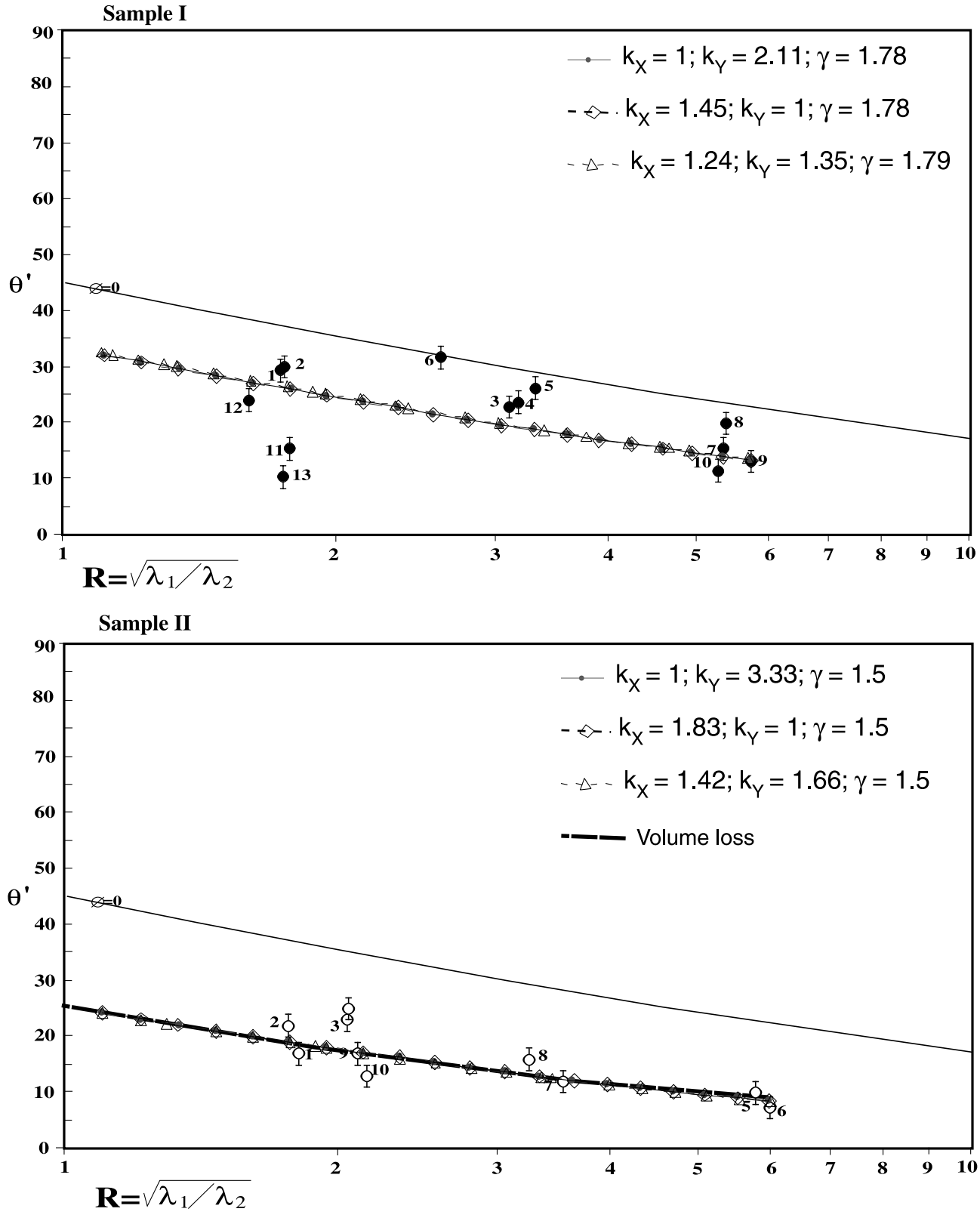

Fig. 16. $R - \theta'$ plots for samples I and II and the paths from two-dimensional modeling of progressive deformation.

becomes:

$$\mathbf{D} = \begin{bmatrix} k_x & 0 & \Gamma_{xz} \\ 0 & k_y & 0 \\ 0 & 0 & k_z \end{bmatrix} \quad (3)$$

The GENERAL SHEAR program is capable of calculating the orientation and geometry of the strain ellipsoids representing intermediate stages of progressive, steady state deformation for a pre-determined combination of pure and simple shearing, thereby providing the corresponding deformation path. Using this program we can calculate deformation paths that match the data on the *xz*-plane, and also match the measured stretch in the *y*-direction. Such strain paths for the two samples are shown in Fig. 16. The 'best fit' paths selected were those that pass through the points representing the most highly deformed rock. These paths also represent reasonably well the less deformed states of strain in the shear zones. This is especially true for sample II. The values of stretch parallel to *x* and *y* for the best fit strain paths k_x and k_y, are shown in Table 1. The value of k_x and k_y given are those that correspond to the highest state of deformation—at the end of the modeled strain paths.

The values of stretch associated with the strain paths and given in Table 1 do not by themselves uniquely define a strain path in the *xz*-section, as represented in Fig. 16. Any number of different combinations of stretches in *x* and *y* can produce identical paths. End member strain paths include volume loss by shortening perpendicular to the shear zone, with no stretch in *y* ($k_x = k_y = 1$); no stretch in *x*, with all the area loss in the *xz*-face compensated for by stretch in *y* ($k_x = 1$; $k_y > 1$) (this corresponds to transpression in the sense of Sanderson and Marchini (1984)); no stretch in *y*, with all the area loss in the *xz*-face compensated for by stretch in *x* ($k_y = 1$; $k_x > 1$). The values of k_x, k_y and volume loss that correspond with each of these end members are shown in Table 1. Although the strain distribution, as represented by the ratio of principal strains and orientations on the *xz*-face, are identical for these various strain paths, the three-dimensional strain pattern is different, and the paths can be distinguished by the stretch in the *y*-direction. This is clearly shown by plotting the data and strain paths on a Flinn diagram (Fig. 17). Consideration of strain ratios in three dimensions shows that extension along both *x* and *y* is required to provide a reasonable match to the data.

4.4. Other constraints on strain

The dimensions of the aggregates on the *xy*-, *yz*-, and *xz*-planes, as distinct from the aspect ratios used in the strain analysis, provide an additional and independent means of discriminating among possible strain paths. The various paths that produce identical values of strain ratio and orientation on the *xz*-plane (Fig. 14) involve differences in strain magnitude and hence size of the aggregates in different sections and directions.

In particular, it is useful to consider the length of the aggregates in the *y*-direction. If there is any true stretch in the *y*-direction it will show up in the *yz*-plane as a change in the length of the aggregates across the shear zone. Shear strain in the *xz*-plane makes no contribution to the dimension of the aggregates in *y*, which is always a direction of principal strain in the models considered. In Fig. 18, the average lengths of the aggregates in *y* in a traverse across the shear zone in sample I are plotted. The aggregates are up to 20% longer in the center of the shear zone than at the margins. This implies a 'true' stretch in the *y*-direction, which is roughly consistent with the value of k_y used in the simulation strain path (Table 1). For sample I, the maximum stretch in *y* is 35% in the best matching simulated strain path. The difference in k_y between the least and most deformed parts of the sample as calculated from the simulated strain path is about 24%, comparable with the 20% stretching apparent in Fig. 18. Similar results are obtained for sample II.

5. Discussion and conclusions

The strain data presented in this paper are necessarily 'noisy', and there are several factors that contribute to the

Table 1
Parameters for modeled strain paths for the Kebnekaise shear zones. Strain parameters representing four different paths involving identical strain patterns in the *XZ*-plane and different absolute values of principal strains and stretches in the *Y*-direction. Only the first path in each case (plane strain + volume loss) corresponds to the classical two-dimensional analysis of shear zones. All the other paths are constant-volume. The values of *k* in columns 3–5 correspond to those at the termination of the deformation path in Fig. 15a and b

Example	Strain pattern	$k_x = k_a$	$k_y = k_b$	k_z	γ
Sample 1	Plane strain + volume loss	1.0	1.0	0.47	1.78
	Shortening across the shear zone, stretch parallel to *Y* (transpression)	1.0	2.11	0.47	1.78
	Shortening across the shear zone, stretch parallel to *X*	1.45	1.0	0.69	1.78
	Shortening across the shear zone, stretch parallel to *X* and *Y*	1.24	1.35	0.60	1.79
Sample 2	Plane strain + volume loss	1.0	1.0	0.30	1.50
	Shortening across the shear zone, stretch parallel to *Y* (transpression)	1.0	3.33	0.30	1.50
	Shortening across the shear zone, stretch parallel to *X*	1.83	1.0	0.55	1.50
	Shortening across the shear zone, stretch parallel to *X* and *Y*	1.42	1.66	0.42	1.50

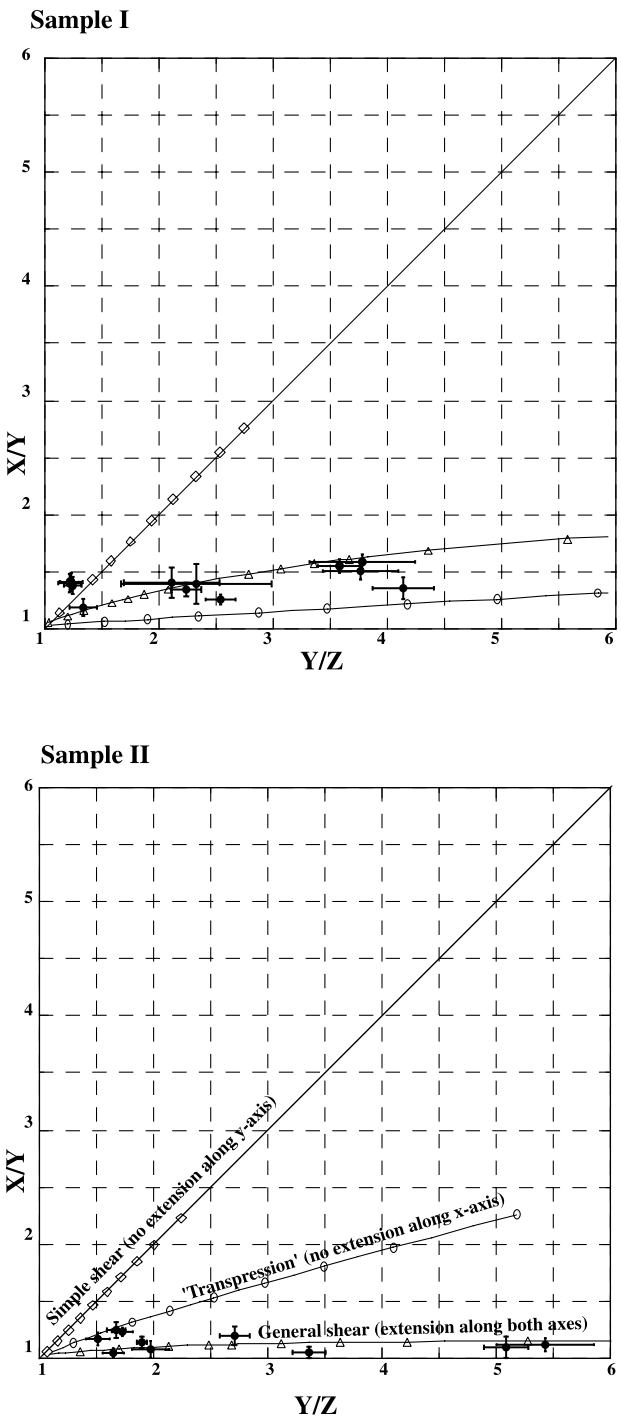

Fig. 17. Flinn diagram with the strain paths shown in Fig. 16.

noise. The aggregates used to record strain are not ideal. First, as in most strain studies, the strain markers used are not originally spherical but rather are irregular, although roughly equant, in shape. This is not a significant drawback provided that indeed there is no primary fabric. Second, it is sometimes difficult to distinguish adjacent strain markers; it is a judgment call as to whether some plagioclase aggregates constitute one or two markers. Third, the domains in which strain is measured are not truly homogeneous; the strain varies continuously across the zones and it is arbitrary where the boundaries between domains are placed. The domains have to be large enough to contain a sufficient number of particles to measure strain, yet small enough to be reasonably represented as a homogeneous domain. Fourth, syn- and perhaps also post-deformational recrystallization acts as a mixing process that blurs the edges of the aggregates by grain neighbor swapping. At very high strains, this may cause the aggregates to disappear altogether. This was not the case with the shear zones studied here, although it was in the previous analysis made by Srivastava et al. (1995). In that study, the central part of the shear zone appeared to be devoid of aggregates, although the minerals were still present in roughly the same proportions as in the marginal zones (Srivastava et al., 1995).

Despite these sources of error and uncertainty, the general pattern of strain is consistent in all shear zones studied, the strains do lie on 'paths' of the kind to be expected in zones of concentrated shear. The three-dimensional strain is clearly of the flattening type. These are not zones of plane strain, simple shear. This conclusion is robust, although the absolute values of strain are poorly constrained.

Inferences based on Fig. 14 alone could lead one to conclude that a progressive loss of volume accompanied the deformation in the shear zones, resulting in about 60% volume loss within the shear band for sample I, and 70–75% volume loss for sample II. This conclusion is, however, in direct conflict with the results of the two independent geochemical analyses (Figs. 11 and 12), which indicate that there has been no significant movement of elements across the shear zone, as would be expected if significant amounts of material had been removed by solution or diffusion. This is the 'volume-loss paradox' noted in the introduction. It should also be noted that the lengths of the aggregates in the *yz*-plane (Fig. 18) are inconsistent with the inference of volume loss based on particle measurement on the *xz*-plane.

We have argued here that the resolution of the paradox lies in consideration of the three-dimensional nature of the strain development in these shear zones. By sectioning the shear zone samples into slabs, we have been able to calculate three-dimensional states of strain across the shear zones. These show clearly that there is indeed flattening strain in the zones (Fig. 9). We can match the recorded three-dimensional strain ratios using a model of progressive simple shearing with stretching in the *x*- or *y*-directions, or

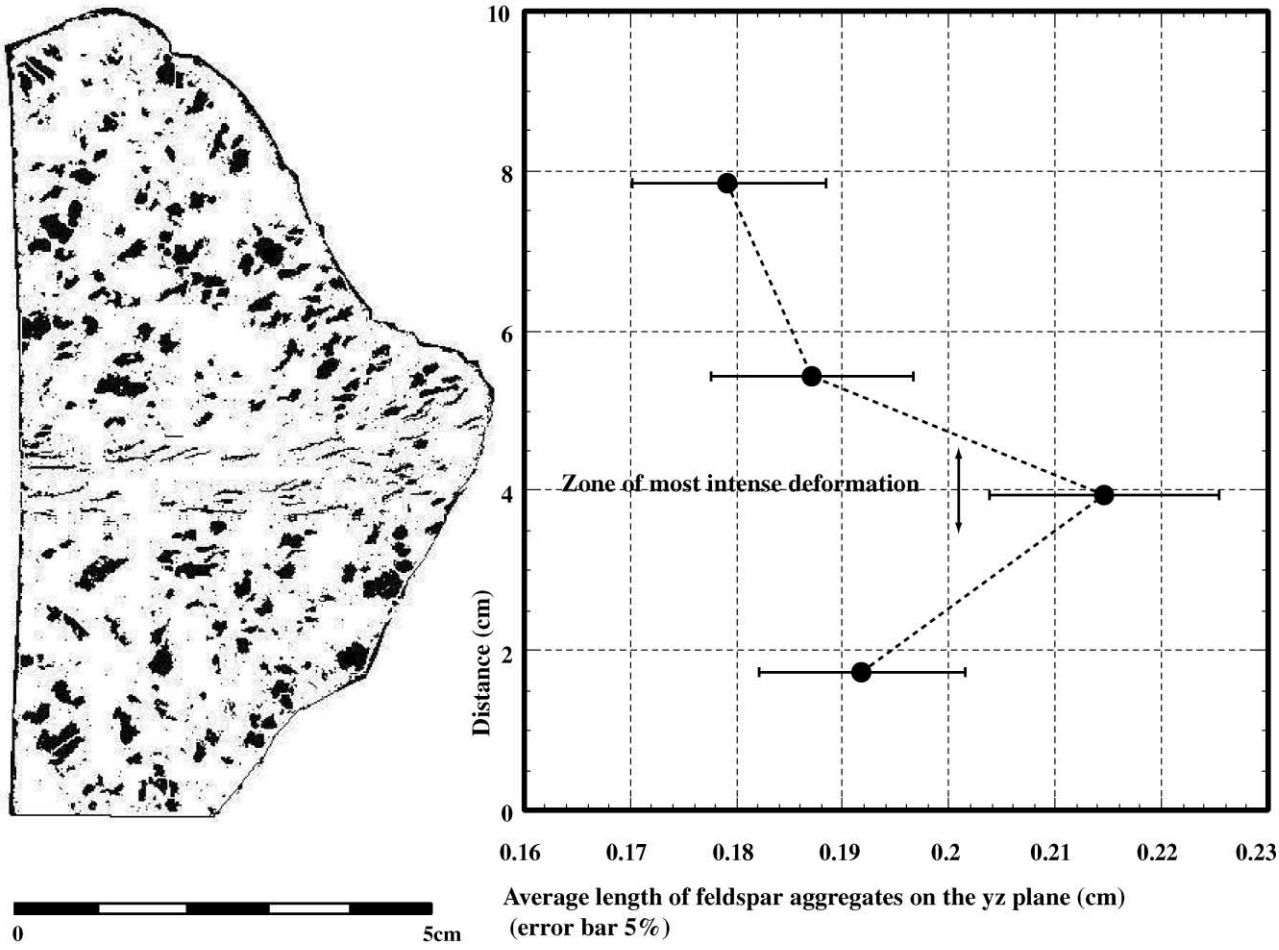

Fig. 18. Differential stretch of the feldspar aggregates in the *y*-direction against distance across the shear zone, plotted for sample I.

both. There are an infinite number of paths that involve volume loss and stretch in x and y in different degrees, all of which produce identical values of strain ratio and orientation on the xz-, and yz- or xy-planes. However, if we add the constraint of no volume change and a fixed total stretch in y, a finite state of strain, represented by a point on the $R - \theta'$ diagram (Fig. 14) or the Flinn plot (Fig. 17), can be reached by a unique strain path involving constant rates of stretching in x and y and simple shear, γ, parallel to the x-direction in the xz-plane. Thus, we can reconcile the three-dimensional strain with a strain path that involves no volume change.

The resolution of the 'volume loss' paradox itself leads to a problem of shear zone geometry. The discussion of strain thus far has assumed deformation occurred in parallel bands, with gradients only allowed in the direction perpendicular to the bands. As pointed out by Hudleston (1999, fig. 4a and b), a component of differential stretching in x or y leads to strain compatibility problems at the boundaries of the shear zones if deformation remains continuous. This is illustrated in Fig. 19. The only way we can accommodate such stretching while maintaining compatibility, is by linking individual shear zones in an anastomosing fashion, as illustrated schematically in Fig. 20. In such an arrangement, the stretch in x and y in an individual band is accommodated by 'extrusion' of material from the shear zone in these directions (as represented schematically in Fig. 19). The establishment of strain gradients in x and y allows for continuity of material, and the anastomosing pattern of shear zones allows the stretches in x and y to be transferred around lozenges of undeformed or weakly deformed rock. If the overall pattern of strain in all the individual shear zones is flattening, then the bulk strain in the rock will also be of the flattening type. If the pattern of interconnection of shear bands is complex, the strain distribution in individual bands may also be expected to be complex (see Fig. 4). A full analysis of this is beyond the scope of the present work, but Figs. 19 and 20 provide a schematic representation of how shear zones might be linked to maintain strain compatibility. The shear zones with strongly flattening strains described in this paper are more likely to represent the 'corners' than the 'sides' of a network of lozenges of the type shown in Fig. 20.

It should be pointed out that the strain paths presented in Figs. 14, 16 and 17 share the property that the rates of stretching in x and y and of shear straining are constant or,

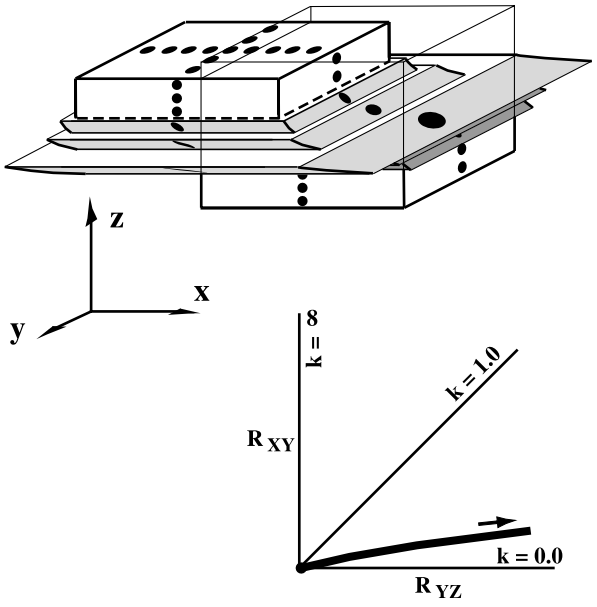

Fig. 19. 'Transpression' in a shear zone with sigmoidal fabric. A shear zone similar to that shown in Fig. 1, with shortening in the *z*-direction, accommodated by extension in *y* and *x*. For the purpose of illustration, deformation is homogeneous in each slice, leading to discontinuities in the shear plane in the *y*- and x-directions. The strain path will be of the flattening type, as illustrated on the Flinn plot.

if variable, they change together such that their ratios are the same. It is likely that in nature there are changes in rates of stretching and shearing that affect different components differently. Also, the deformation paths experienced at different locations along and across a shear zone will not be the same. We do not explore these issues further here. The strain paths inferred for the studied shear zones are at best approximations to what the rocks in the middle sections of the shear zones may have experienced. We have no indication of what the rates of strain might have been.

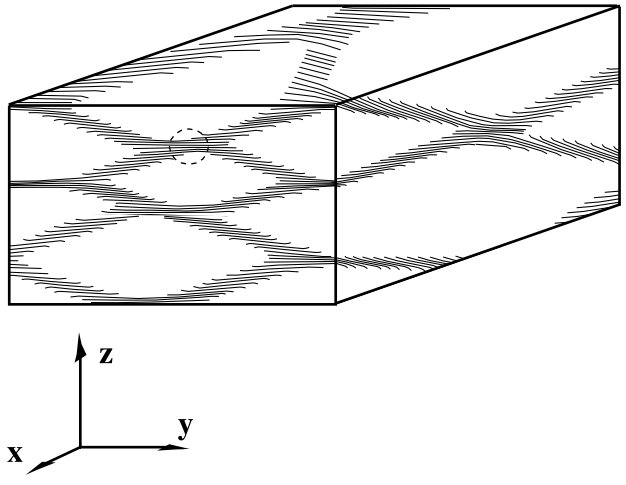

Fig. 20. Schematic illustration of the foliation pattern resulting from a network of shear zones defining prismatic lozenges of undeformed rock (note that the shape of the block does not indicate the shear strain). The bulk shear plane is *xy*, with shear in the *x*-direction. The area circled is where the type of strain fabrics observed in the shear zone samples described in this paper.

The deformation within these shear zones is complex, and no simple model is capable of explaining it and accounting for the anastomosing nature of the shear arrays. However, the results obtained from our three-dimensional strain analyses are consistent with those from geochemical analysis in providing an explanation of deformation in individual zones that involves no loss of volume. It does, however, require stretching in the plane of shear that results in the flattening strains developed.

Acknowledgements

This research was supported by NSF (EAR–9506504). We thank Dr Per Holmlund, the staff of the University of Stockholm field station at Tarfala and Erin Young for providing support in the field. We also gratefully acknowledge Drs B. Tikoff and O. Svenningsen for valuable comments and discussions. Finally, we thank journal reviewers C.J. Northrup and H. Sjöström for their constructive reviews and suggestions.

References

Andréasson, P.G., Gee, D.G., 1989. Bedrock geology and morphology of the Tarfala area, Kebnekaise Mts, Swedish Caledonides. Geografiska Annaler 71, 235–239.

Bhattacharyya, P., Hudleston, P.J., Whitney, D.L., 1999. Pressure–temperature conditions of deformation and fluid infiltration of sheared garnet amphibolites. Geological Society of America Abstracts with Programs 31, 168.

Choukroune, P., Gapais, D., 1983. Strain pattern in the Aar Granite (Central Alps); orthogneiss developed by bulk inhomogeneous flattening. Journal of Structural Geology 5, 411–418.

Coward, M.P., 1976. Strain within ductile shear zones. Tectonophysics 34, 181–197.

Coward, M.P., Potts, G.J., 1983. Complex strain patterns developed at frontal and lateral tips to shear zones and thrust zones. Journal of Structural Geology 5, 383–399.

Dallmeyer, R.D., Andréasson, P.G., Svenningsen, O., 1991. Initial tectonothermal evolution within the Scandinavian Caledonide Accretionary Prism: constraints from 40Ar/40Ar mineral ages within the Seve nappe Complex, Sarek Mountains, Sweden. Journal of Metamorphic Geology 9, 203–218.

De Paor, D.G., 1990. Determination of the strain ellipsoid from sectional data. Journal of Structural Geology 12, 131–137.

Fossen, H., Tikoff, B., 1993. The deformation matrix for simultaneous simple shearing, pure shearing, and volume change, and its application to transpression/transtension tectonics. Journal of Structural Geology 15, 413–422.

Gapais, D., Bale, P., Choukroune, P., Cobbold, P.R., Mahjoub, Y., Marquer, D., 1987. Bulk kinematics from shear zone patterns; some field examples. Journal of Structural Geology 9, 635–646.

Gee, D.G., Zachrisson, E., 1979. The Caledonides in Sweden, Sveriges Geologiska Undersökning, C 769, 48pp.

Gee, D.G., Kumpulainen, R., Roberts, D., Stephens, M.B., Thon, A., Zachrisson, E., 1985. The Scandinavian Caledonides. Tectonostratigraphic Map, Sveriges Geologiska Undersökning, Ser. Ba NR 35.

Graham, C.M., Powell, R., 1984. A garnet–hornblende geothermometer:

calibration, testing and application to the Pelona Schist, Southern California. Journal of Metamorphic Geology 2, 13–31.

Grant, J.A., 1986. The isocon diagram—a simple solution to Gresens' equation for metasomatic alteration. Economic Geology 81, 1976–1982.

Gresens, R.L., 1967. Composition-volume relationships for metasomatism. Chemical Geology 2, 47–65.

Hanmer, S., Passchier, C.W., 1991. Shear-Sense Indicators: A Review. Geological Society of Canada Paper 90-17, 72pp.

Hudleston, P.J., 1977. Progressive deformation and development of fabric across zones of shear in glacial ice. In: Saxena, S., Bhattacharji, S. (Eds.). Energetics of Geological Process. Springer-Verlag, New York, pp. 121–187.

Hudleston, P.J., 1999. Strain compatibility and shear zones: is there a problem? Journal of Structural Geology 21, 923–932.

Kanagawa, K. 1990. MacStrain. Strain analysis programs for Macintosh™ II series computers.

Kohn, M.J., Spear, F.S., 1989. Empirical calibration of geobarometers for the assemblage garnet + hornblende + plagioclase + quartz. American Mineralogist 74, 77–84.

Kulling, O., 1964. Översikt över norra Norbottensfjällens Kaledonberggrund, Sveriges Geologiska Undersökning, Ba 19, 166pp.

Law, R.D., 1990. Crystallographic fabrics: a selective review of their applications to research in structural geology. In: Knipe, R.J., Rutter, E.H. (Eds.). Deformation Mechanisms, Rheology and Tectonics. Geological Society Special Publication 54, pp. 335–352.

Lister, G.S., Williams, P.F., 1979. Fabric development in shear zones: theoretical control and observed phenomena. Journal of Structural Geology 1, 283–297.

Lloyd, G.E., Law, R.D., Mainprice, D., Wheeler, J., 1992. Microstructural and crystal fabric evolution during shear zone formation. Journal of Structural Geology 14, 1079–1100.

Mawer, C.K., 1983. State of strain in a quartzite mylonite, Central Australia. Journal of Structural Geology 5, 401–409.

Means, W.D., 1990. Kinematics, stress, deformation and material behavior. Journal of Structural Geology 12, 953–971.

Moecher, D.P., Essene, E.J., Anovitz, L.M., 1988. Calculation and application of clinopyroxene–garnet–plagioclase–quartz geobarometers. Contributions to Mineralogy and Petrology 100, 92–106.

Mohanty, S., Ramsay, J.G., 1994. Strain partitioning in ductile shear zones: an example from a Lower Pennine nappe of Switzerland. Journal of Structural Geology 9, 635–646.

Owens, W.H., 1984. The calculation of a best-fit ellipsoid from elliptical sections on arbitrarily oriented planes. Journal of Structural Geology 6, 571–578.

Panozzo, R., 1987. Two-dimensional strain determination by the inverse SURFOR wheel. Journal of Structural Geology 7, 115–119.

Passchier, C.W., Urai, J.L., 1988. Vorticity and strain analysis using Mohr diagrams. Journal of Structural Geology 10, 755–763.

Powell, R., 1985. Regression diagnostics and robust regression in geothermometer/geobarometer calibration: the garnet–clinopyroxene geothermometer revisited. Journal of Metamorphic Geology 3, 231–243.

Ramberg, H., 1975a. Superposition of homogeneous strain and progressive deformation in rocks. Bulletin of the Geological Institutions of the University of Uppsala, New Series 6, 35–67.

Ramberg, H., 1975b. Particle paths, displacement and progressive strain applicable to rocks. Tectonophysics 28, 1–37.

Ramsay, J.G., Allison, I., 1979. Structural analysis of shear zones in an alpinised Hercynian granite (Maggia Lappen, Pennine Zone, Central Alps). Schweizerische Mineralogische und Petrographische Mitteilungen = Bulletin Suisse de Mineralogie et Petrographie 59, 251–279.

Ramsay, J.G., Graham, R.H., 1970. Strain variation in shear belts. Canadian Journal of Earth Sciences 7, 786–813.

Ramsay, J.G., 1980. Shear zone geometry: a review. Journal of Structural Geology 2, 83–99.

Sanderson, D., Marchini, R.D., 1984. Transpression. Journal of Structural Geology 6, 449–458.

Schwerdtner, W.M., 1982. Calculation of volume change in ductile band structures. Journal of Structural Geology 4, 57–62.

Simpson, C., 1983. Strain and shape fabric variations associated with ductile shear zones. Journal of Structural Geology 5, 61–72.

Srivastava, H.B., Hudleston, P., Earley, D., 1995. Strain and possible volume loss in a high-grade ductile shear zone. Journal of Structural Geology 17, 1217–1231.

Tikoff, B., Fossen, H., 1993. Simultaneous pure and simple shear: the unified deformation matrix. Tectonophysics 217, 267–283.

Tikoff, B., Teyssier, C., 1994. Strain modeling of displacement field partitioning in transpressional orogens. Journal of Structural Geology 16, 1575–1588.

Wallis, S.R., 1992. Vorticity analysis in metachert from the Sanbagawa Belt, SW Japan. Journal of Structural Geology 14, 271–280.

Wheeler, J., 1986. Average properties of ellipsoidal fabrics: implications for two- and three-dimensional methods of strain analysis. Tectonophysics 126, 259–270.